

# Enhancing Polyimide's Water Barrier Properties through Addition of Functionalized Graphene Oxide

*Samuel Hocker,<sup>†</sup> Natalie Hudson-Smith,<sup>§</sup> Hannes C. Schniepp,<sup>†</sup> David E. Kranbuehl<sup>§,\*</sup>*

<sup>§</sup> Department of Chemistry, The College of William & Mary, Williamsburg, VA, USA

<sup>†</sup> Department of Applied Science, The College of William & Mary, Williamsburg, VA, USA

## **ABSTRACT**

Graphene oxide produced by Tour's method (GO) and GO functionalized with 4-4' oxydianiline (ODAGO) are incorporated at 0.01 to 0.10 weight percent (wt%) into a polyimide (PI) made from 3,3'-benzophenonetetracarboxylic dianhydride (BTDA) and 4-4' oxydianiline (ODA). The performance properties of these two systems GO-PI and ODAGO-PI at extremely low GO concentrations are compared. ODAGO-PI nanocomposite's performance properties are comparable to previous results citing concentrations 10 times higher and displayed significantly greater improvement than unfunctionalized GO-PI films. The 0.01 wt% ODAGO-PI film demonstrated a factor of ten decrease in water vapor permeability. The 0.10 wt% ODAGO-PI film displayed the maximum increase of 82% in Young's modulus. The water vapor permeability results were fit to the Nielsen law. We found that the model yielded unphysically large aspect ratios for the 0.01 wt% ODAGO-PI, 100 times larger than the AFM-measured value. For the GO-PI, we observe less enhancement of the barrier properties. The large aspect ratio

indicates tortuosity effects alone cannot explain the enhanced barrier properties. We propose that the improved barrier properties are also due to a stabilizing effect of the flakes on the polymer matrix, where reduced mobility of the PI chain reduces diffusion through the polymer matrix.

ATR-FTIR, WAXS, Raman and  $T_g$  results support this view.

## INTRODUCTION

Polyimides (PI) are a family of high-performance polymers that derive excellent mechanical strength, thermal resistance, and chemical resistance from their stable and stiff imide bonds. As a result, polyimides can be found in a wide array of industrial applications such as electric motors, jet engine blades, aircraft wire, and molded pistons and seals. Recent aerospace applications of PI films include the Mars Explorers Curiosity and Spirit [1], the European Space Agency's Rosetta space probe [2], and the sun shield of NASA's James Webb Space Telescope [3]. In all of the PI applications efficiency can be improved by using less material to effect the same utility. Additionally, in some cases, the use of PI can enable new applications or technologies in extreme environments, e.g. outer space. In a global effort to make better and enabling materials, many different fillers and nano-fillers have been researched for polyimide composites and nano-composites. In recent years, graphene has been researched as a nano-filler to make polyimide nanocomposites with new and advantageous properties.

Research in graphene-PI nanocomposites has been motivated by lending graphene's extremely high modulus of 1 TPa, ultimate strength of 130 GPa, gas impermeable honeycomb network, and high electrical and thermal conductivity [4] to the polymer matrix. A challenge in creating graphene-polymer nanocomposites is graphene's extremely hydrophobic and chemically unreactive pristine carbon-honeycomb structure. It is difficult to disperse graphene single layer nano-sheets into the polar solvents typically used for polymerization and synthesis.

The increased interest in graphene's exceptional properties has revitalized interest in an analogous polar compound, graphene oxide (GO). GO has the same honeycomb structure as graphene but with oxygen-containing functional groups on the surface of the planar structure.

These oxygen-containing functional groups are ketones, 6-membered lactol rings, alcohols, epoxides and hydroxyl groups [4]. First produced in 1859 by Brodie [5] and later by Hummers Jr. and Offeman [6], graphitic oxide can be dispersed into water or organic solvents commonly used in polymer precursor resins to create GO-polymer composite materials [4]. A wide range of GO-polymer nanocomposites have been researched previously for polyurethanes, nylons, and many other polymers including several PI systems, with as many variations on GO synthesis, functionalization, and composite fabrication technique [4, 7-17]. Many GO-PI works show improvements in Young's modulus [18-20], tensile strength [18, 20], gas barrier properties [19, 21], electrical conductivity [19, 20, 22], and decreases in thermal stability [19, 22].

Regarding tensile modulus and strength improvements published on loading GO into PI: Wang, Yang [23] used loadings of 0.3 to 5 wt% and found a maximum 1400% increase in tensile modulus and a 990% increase in tensile strength for GO sheets functionalized with 4-4' oxydianiline (ODA) in a PI of the monomers 3,3,4,4-benzophenonetetracarboxylic dianhydride (BTDA) and ODA. Tseng, Liao [24], used very low loadings of GO in a PI of bicyclo[2.2.2]oct-7-ene-2,3,5,6-tetracarboxylic dianhydride and ODA, between 0.001 and 0.01 wt% to effect 66% improvement in the tensile modulus while maintaining optical transparency. Shi, Li [18] found an increase of tensile strength by 29% and Young's modulus by 25% with an addition of 0.12% by weight GO in a PI system comprised of 4,4'-bisphenol A dianhydride, 4-4'-oxydiphthalic anhydride and diaminophenyl methane. Zhu, Lim [19] found an increase of the Young's modulus by 282% in a 30% by weight GO-PI system comprised of the monomers pyromellitic dianhydride and ODA. Park, Kim [20] found an increase of 172% in the modulus and an 64% increase in tensile strength with the addition of 0.5 wt% of surface functionalized GO in PI system compromised of pyromellitic dianhydride and ODA. Qian, Wu [25] with a PI of 3,3,4,4-

Biphenyl tetracarboxylic dianhydride and ODA monomers showed a 79% improvement in the tensile strength and a 132% increase in the tensile modulus are achieved by adding 1.5 wt% 3-aminopropyltriethoxysilane functionalized GO. Wang, Lan [26] loaded 3 wt% amino functionalized GO into PI of 3,3',4,4'-Biphenyl tetracarboxylic dianhydride and p-phenylenediamine monomers to effect 63% increase in modulus and 55% increase in the tensile strength. Over the past few years, papers have reported on the increased effect on mechanical performance properties by functionalizing the surface of GO. A few papers have focused on comparing the effect of different functionalizing procedures on the improvement on performance properties, primarily in epoxies[27-30] and in polyimides[20, 31-33].

Regarding gas barrier properties of GO loaded PI films: Zhu, Lim [19] determined that incorporation of GO nano-sheets from 1 to 30 wt%, reduced the oxygen transmission rate through the PI film with a maximum reduction of 93%. Lim, Yeo [31] report a reduction in oxygen permeability of a factor of 95% at 0.5% by weight and a reduction of >99% at 5 wt%. Park, Kim [20] using 2 wt% iodo-functionalized GO found a 73% decrease of water vapor transmission in their PI system. Tseng, Liao [24] at the very low GO loadings of 0.001 to 0.01 wt% found a maximum of 90% decreased water vapor transmission rate in the GO-PI nanocomposite. Kwon and Chang [34] investigated the gas permeability of GO-PI and organically modified hectorite clay, and functionalized hexadecylamine-graphene sheets. They found that from 3 to 20 wt% loadings of functionalized hexadecylamine-graphene sheets in PI of 4,4'-biphenyl tetracarboxylic dianhydride (BPA) and bis(4-aminophenyl) sulfide (APS), the oxygen transmission decreased 48% to 92%, respectively. From this brief literature review of GO-PI and functionalized GO-PI nanocomposite it is clear that the gas or water vapor permeability and

tensile properties are improved, but the properties vary according to the polyimide used and the surface chemistry of the graphene oxide.

In order to understand the molecular interactions between the polymer and GO that lead to gas permeability and tensile improvements, two types of GO-PI composite films are synthesized with very low 0.01, 0.03, 0.06, and 0.1 wt% GO loadings. The loading of 0.01 wt% is a factor of ten lower GO-PI loading than the commonly used particle loadings in polymers. The two types of GO-PI composites synthesized differ in their GO surface chemistry. The first type uses as produced GO and then was thermally reduced during in-situ PI synthesis at 300 °C [33]. In the second type, GO was reacted with the ODA monomer to make ODAGO prior to being added to the polyamic acid resin and thermally imidized at 300 °C to become ODAGO-PI.

The differing effect on performance properties of functionalized versus un-functionalized is explored for the first time at these very low concentrations through water vapor barrier, water uptake, and tensile measurements on both types of composites. The variation in improvement of the GO composite's properties presents a systematic comparison of the effect of functionalized GO on composite properties. The results show the important fact that large improvements can be found in the performance properties at these much lower loadings of GO, as low as 0.01 wt%, and that use of functionalized GO produces significantly greater improvements than the widely used as-produced GO. Additionally, we identify the effect of hydrogen bonding between the nano-sheets and the polymer matrix. This bonding stiffens the polymer chains, decreasing gas permeability and increasing the tensile modulus beyond the usual effect of GO's high aspect ratio sheet structure and high modulus.

## **EXPERIMENTAL METHODS**

### ***GO Synthesis and Dispersion***

GO is obtained by the synthesis procedure of Hummers[6]. Dry GO flakes were massed and added to a flask of DMAc. This mixture was bath sonicated in water using a Fisher Scientific FS110D sonicator for 30 minutes to result in a homogenous GO-DMAc dispersion. To perform topographical characterization of the exfoliated flake height, we first utilized the Laurell WS-400Bz-6NPP-Lite Spin Processor to disperse samples of each dispersion onto freshly cleaved muscovite mica substrates (Ted Pella, PELCO®, Grade V5). Then, we used two atomic force microscopes (Bruker, MultiMode and NT-MDT, NTEGRA) to perform dynamic-mode scans of the substrates, obtaining height data on individual flakes.

### ***Functionalization of GO Particles with ODA***

Under nitrogen, an ODA-DMAc solution was added to a GO-DMAc dispersion at a ratio of 15 mmol ODA per gram of GO. The ODA reacted with the GO under a nitrogen flush 60 °C reflux for 24 hours to yield a dispersion of functionalized GO, designated ODAGO.

### ***Polyimide Synthesis***

The polyimide precursor, poly(amic acid)(PAA), was prepared from the monomers benzophenone-3,3', 4,4'-tetracarboxylic dianhydride (BTDA) and 4-4' oxydianiline (ODA). Prior to use, BTDA was dried in a vacuum oven at 150 °C for 5 hours. Equimolar amounts of ODA and dry BTDA are independently dissolved into dimethylacetamide (DMAc) to make two solutions. The dissolved BTDA is added to a three-necked resin flask, followed by the ODA solution. The reaction is stirred at room temperature under nitrogen for 48 hours. The resulting

poly(amic acid) resin (PAA) was obtained at 12 wt% solids in DMAc and was used for the synthesis of both unloaded and loaded PI composite films[35].

An even layer of PAA was spread into a soda lime glass petri dish and this dish of PAA was then placed into a Thermolyne 47900 Furnace to obtain a solid PI film. Thermal cure was a ramp to 100 °C with a one hour isotherm followed by a 2 hour ramp to 300 °C with a one hour isotherm, and returned back to room temperature. The PI film was easily peeled from the glass and characterized[35].

### ***GO Nanocomposite Synthesis***

A solvent mixing technique was used to make the ODAGO-PI and GO-PI. The GO-DMAc dispersion was mixed with the PAA to make GO-PAA. ODAGO-DMAc was mixed with the PAA to make ODAGO-PAA. GO and ODAGO were added at 0.01, 0.03, 0.06 and 0.10 wt% per PAA solids. The GO-PAA and ODAGO-PAA were spread into petri dishes and subjected to the same cure cycle used to produce the PI films.

### ***Wide Angle X-Ray Diffraction (WXR)***

Wide angle X-Ray diffraction data were collected on a Bruker SMART Apex II three circle diffractometer system with graphite monochromator, Cu K $\alpha$  fine-focus sealed tube ( $\lambda = 1.54178 \text{ \AA}$ ) and CCD collector using  $\varphi$  and  $\omega$  scans[36].

### ***Water Vapor Transmission, Permeability***

Water vapor transmission rates were measured using ASTM E96-95: Methods for Water Vapor Transmission of Materials. Samples were cut by hand into approximately 1.5 cm squares. Thickness dimensions of approximately 0.05 mm were measured with a iGaging EZ-Cal digital micrometer.

For each sample, a cylindrical vial was filled to approximately 75% capacity with the desiccant Drierite with color indicator (Acros Organics). Per vial, the rim was coated with silicon vacuum grease. A square sample of the PI films was placed on top of each vial rim and the vacuum grease created a seal between the PI film and the glass to prevent water vapor passage. The vials were placed in a 70% humidity sealed environment at 23 °C. Following ASTM E96-95, the mass of each vial was measured over time. The rate of change of mass versus time was used to calculate our relative water vapor transmission rate. Three to seven samples were measured at each weight percent, the averages and standard deviations were reported. Measurements were also made on Kapton Type HN 25 μm film and the DuPont reported permeability value was used as a standard when we converted water vapor transmission rates to permeability[37].

### ***Water Gain Analysis***

The rate of water absorption was determined using the procedure designated in ASTM D750- 98 standard test: Method for Water Absorption of Plastics. PI samples were cut into 1 × 3 cm strips with an average thickness of 50 μm. The strips were left in a 100 °C oven for an hour prior to immersing in water to remove any deposited ambient humidity. The strips were then submerged in deionized water and kept at 23 °C. Measurements were made on three to five samples and the averages and standard deviations were reported.

### ***Mechanical Testing***

A TA Instruments AR 100 instrument was fitted with adjustable film grips to follow ASTM D882-73. The tensile stress/strain plots were produced to obtain Young's modulus on 5 to 15 samples. Averages and standard deviations were calculated and reported.

*Attenuated total reflectance Fourier transform infrared spectroscopy (ATR FTIR)*

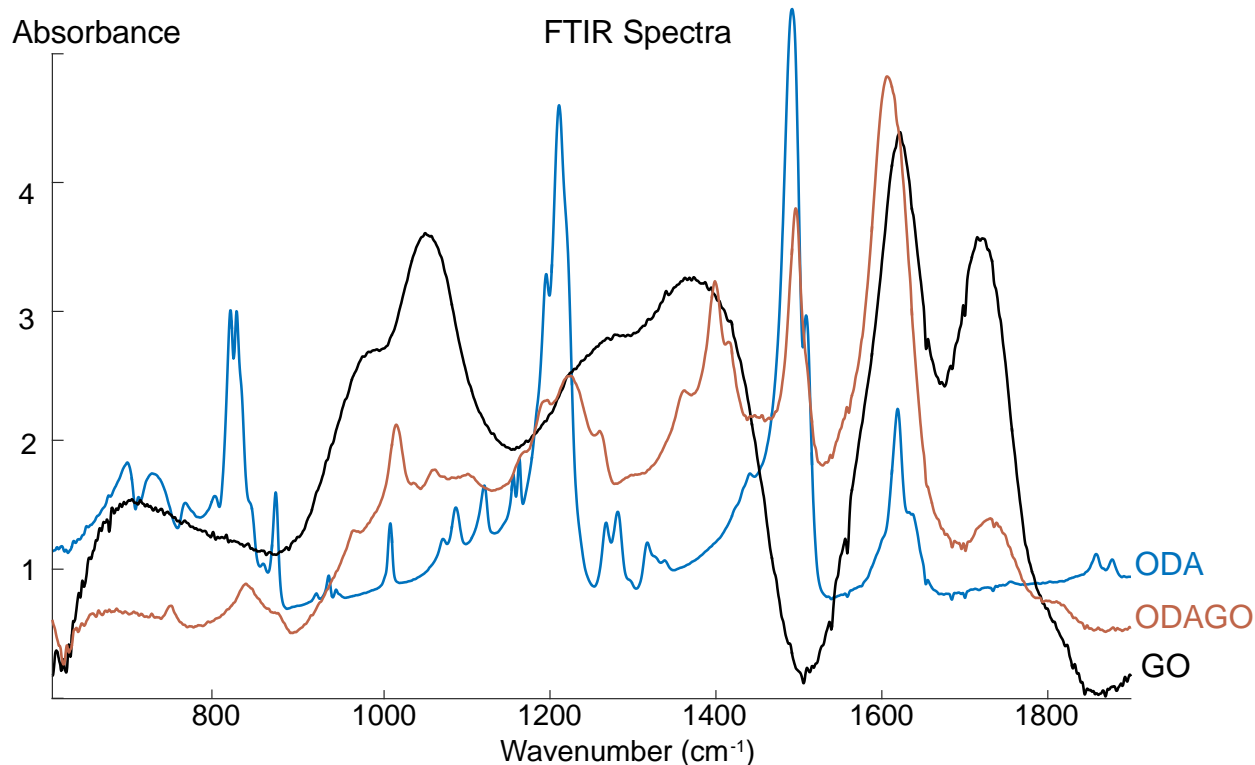


Figure 1: ATR-FTIR normalized absorbance spectra of ODA, ODA-GO<sub>i</sub> and GO<sub>i</sub>.

Samples of ODAGO were prepared for ATR-FTIR by taking an aliquot of the ODAGO-DMAc dispersion and adding isopropyl alcohol drop wise until the ODAGO particles precipitated out of suspension. The precipitated dispersion was centrifuged at 5000 RPMs for 10 minutes in a Universal 320 Centrifuge. The supernatant was poured off and 5 mL of DMAc was added to dissolve any unreacted ODA. The centrifugation and DMAc washing was repeated three times. After the third wash, the ODAGO solids were removed and dried in a 55 °C vacuum oven at 23inHg for 48 hours. Dry, solid ODA-GO spectra from 600 to 4000 cm<sup>-1</sup> were obtained using the IRTracer-100 Shimadzu FTIR's MIRacle 10 Single Reflectance ATR Accessor.

The spectra are shown in Figure 1. For the unreacted GO spectrum, characteristic peaks include 1050, 1620 and 1720-30 cm<sup>-1</sup>. The 1050 peak is a C-O vibration of an epoxy group. The

1620 peak is the C=C stretch along the graphene plane. The 1720-1730 peak is the C=O stretch. Unique to the ODAGO spectrum, the new peak at 1390 is the amide III peak that indicates amide bonds are formed in the ODAGO. In addition, there is a new peak at  $743\text{cm}^{-1}$ , not seen in the ODA nor in the GO, which is the N-H stretch of an amide bond. Further the alkoxide/epoxide peak in the GO spectrum at 1050 is absent in the ODAGO spectrum showing the epoxide groups have reacted. On the graphene surface, the amine groups of ODA monomer are expected to react first with the epoxy groups as that peak is absent in the ODAGO, followed by reactions with the less reactive oxide groups such as C=O. The carboxylic group 1732 peak in the ODAGO was reduced in height compared with the peak in the GO. In summary, the appearance of amide peaks as well as peaks absent in the ODAGO spectra compared to the reagents used for its synthesis indicate that the ODA chemically reacted with the GO and functionalization was successful.

## Atomic Force Microscopy of GO and ODAGO Nano-sheets

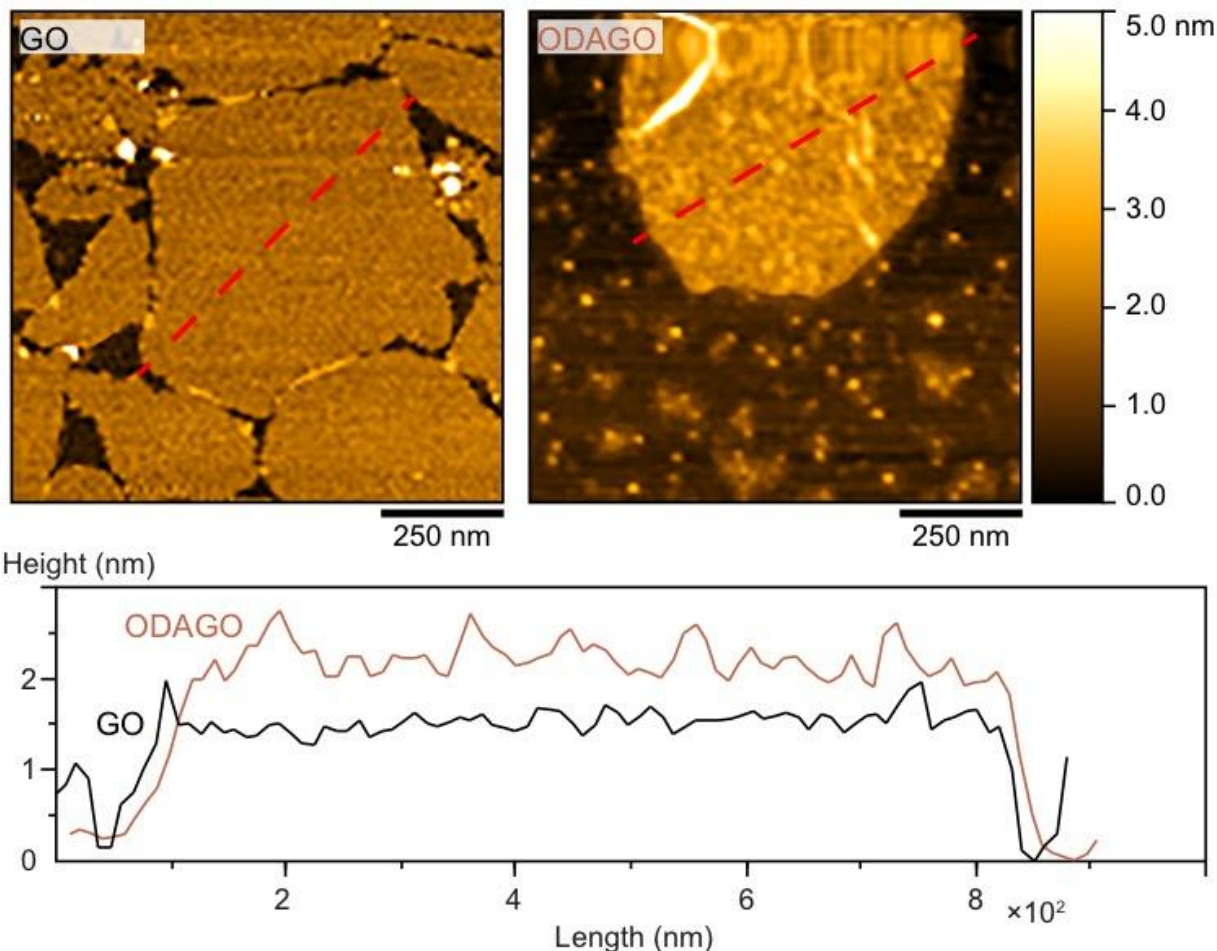


Figure 2: Atomic force microscope images and profiles of graphene oxide (GO) and ODA functionalized graphene oxide (ODAGO).

High resolution atomic force microscopy (AFM) images of the GO and ODAGO sheets are shown in Figure 2. The range of lateral diameters for GO flakes was observed to be 300 to 1200 nm with most GO observed to be ~800 nm. From the profile, ODAGO is approximately 0.5 nm to 1 nm thicker than GO. The functionalized surface is observed to much rougher in Figure 2 than GO due to the ODA monomer.

## Raman Spectra

Raman measurements were performed on an inverted microscope (Nikon, TiU) with a laser wavelength of 632.8 nm from a HeNe laser (Research Electro-Optics, LHRP-1701) with an

excitation power of 2 mW. The laser was filtered (Semrock, LL01-633-25) and focused to the sample using a 20× objective (Nikon CFI, N.A. = 0.5). Scattering from the sample was filtered (Semrock, LP02-633RS-25) and focused to the entrance slit of the spectrograph (Princeton Instruments, SP2356, 600 g mm<sup>-1</sup> grating blazed at 500 nm). The observed Raman frequencies were calibrated using a cyclohexane standard[38].

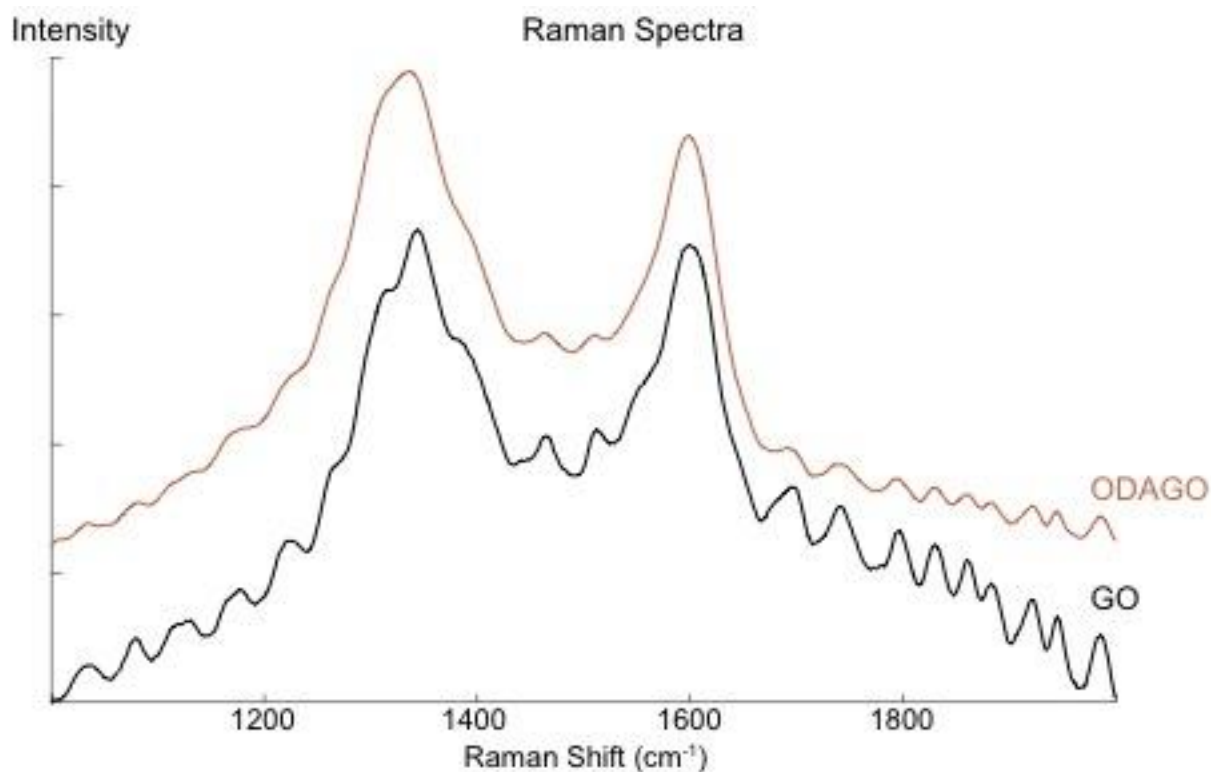


Figure 3: Raman Spectra of GO and ODAGO.

The so-called D and G peak intensities ( $I_D$  and  $I_G$ ) of the Raman spectra peaks of 1350 and 1600 cm<sup>-1</sup> respectively, can be related to the integrity of the GO honeycomb carbon lattice. The G peak is associated with sp<sup>2</sup> hybridized carbon of the carbon honeycomb lattice. The D peak relates to sp<sup>3</sup> hybridized carbon, and is associated with defects in the graphene carbon lattice[39]. The measured  $I_D/I_G$  ratio for GO is 1.03 and the  $I_D/I_G$  ratio for ODAGO is 1.16, in Figure 3. Since the  $I_D/I_G$  ratios remain similar after functionalization with ODA, the Raman

confirms that the impermeable GO honeycomb carbon lattice is maintained for the ODAGO nano-sheets.

## RESULTS AND DISCUSSION

### Permeability

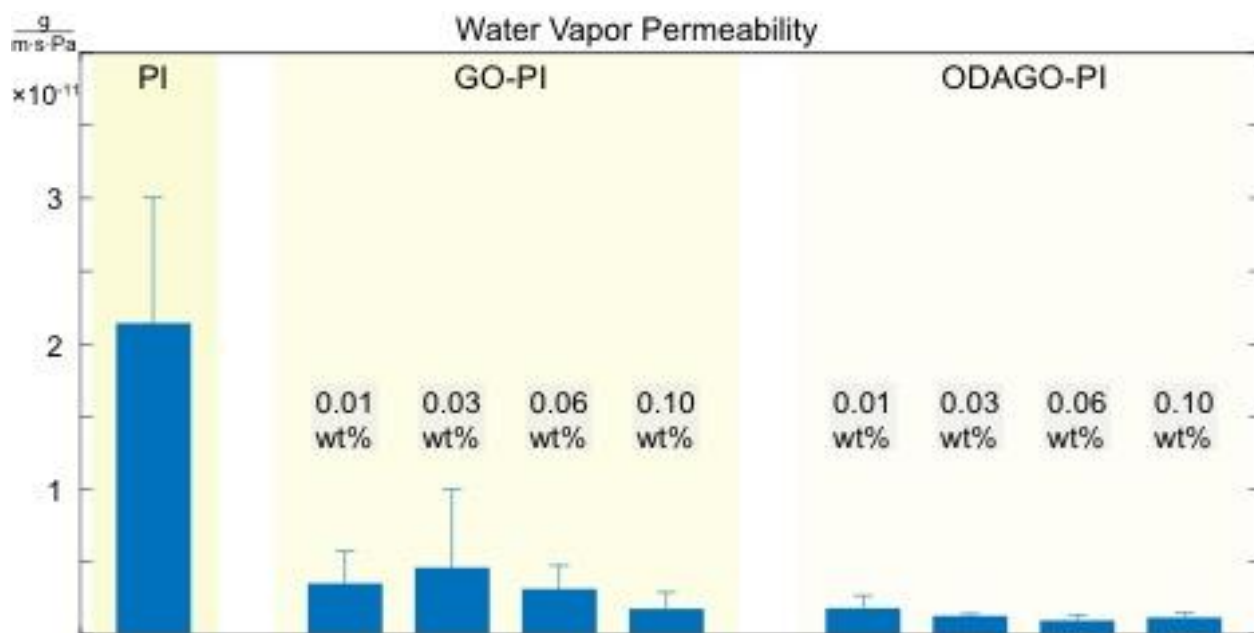


Figure 4: Water vapor permeability for unloaded PI, GO-PI, and ODAGO-PI films at 23 °C and 70% humidity.

Water vapor permeability was significantly reduced as a result of incorporation of functionalized ODAGO compared to un-functionalized GO nano-particles in the PI matrix. A plot of permeability versus PI composition is shown in Figure 4. The functionalized ODAGO-PI has a two to threefold greater reduction in water vapor or permeability than GO-PI samples. The ODAGO-PI composite films had a ten-fold reduction in water vapor transmission compared to the neat PI film. The 0.1 wt% ODAGO-PI films had the highest reduction in water vapor permeability, over a factor of ten compared to the unloaded PI film.

GO-PI films also reduced water vapor transmission but were less effective at preventing water vapor transmission as ODAGO-PI films. At 0.01 wt%, the GO-PI film demonstrated a 5-fold reduction of water vapor transmitted compared to the neat system. The 0.1 wt% GO-PI had

a 10-fold reduction in water vapor transmission compared to the neat sample. The 0.1 wt% GO-PI has a greater permeability than 0.01 wt% ODAGO-PI but the ODAGO-PI composite achieves this reduction at a 10-fold lower loading than the GO-PI film.

Previous work done by Zhu et al. while studying oxygen transmission rate of a different PI film GO nanoparticle system showed a 73% decrease of water vapor transmission by inclusion of iodo-functionalized GO sheets at 0.2 and 1 wt% . This 73% at double to ten times our GO percent loading compares to our 90% reduction in ODAGO-PI. Recently, Tseng et al[24] report a water vapor transmission reduction of 91% at 0.01 wt% GO loading and a decrease of 83% in water vapor transmission by inclusion of 0.0001 wt% GO in a different PI matrix. Our results and those of Tseng show the potential for very large reductions in water vapor transmission at very low GO nanoparticle concentrations, especially when compared with previous results on gas transmission for polymer nano composites containing organo-clay[34, 40]. Most important, our results demonstrate that very low GO concentrations show a 2 to 3-fold decrease in water vapor transmission using functionalized GO compared to un-functionalized GO.

To explain and expand upon the surprising effect of the nanosheets on the water vapor permeability, the results were analyzed using the Nielsen equation for describing the tortuosity effect for a polymer filled with plate-like particles[41]. The Nielsen equation can be used to calculate the effective aspect ratio of the particles in the composite from the decrease in the permeability,

$$P_c = \frac{P_f(1 - V_f)}{(1 + (a/2)V_f)}$$

Here  $P_c$  is the composite permeability,  $P_f$  is the neat film permeability,  $V_f$  is the nanoparticle volume fraction, and  $a$  is the aspect ratio, where the diameter (D) of the nanoparticle is divided by the thickness (T). Figure 5 shows the nanoparticle aspect ratios calculated for the GO and ODA GO films. Using an approximate diameter of 800 nm and thickness of 1.5 nm for the GO and 2 nm for the ODAGO, their expected aspect ratios are 530 and 400 to compare with the Nielsen model.

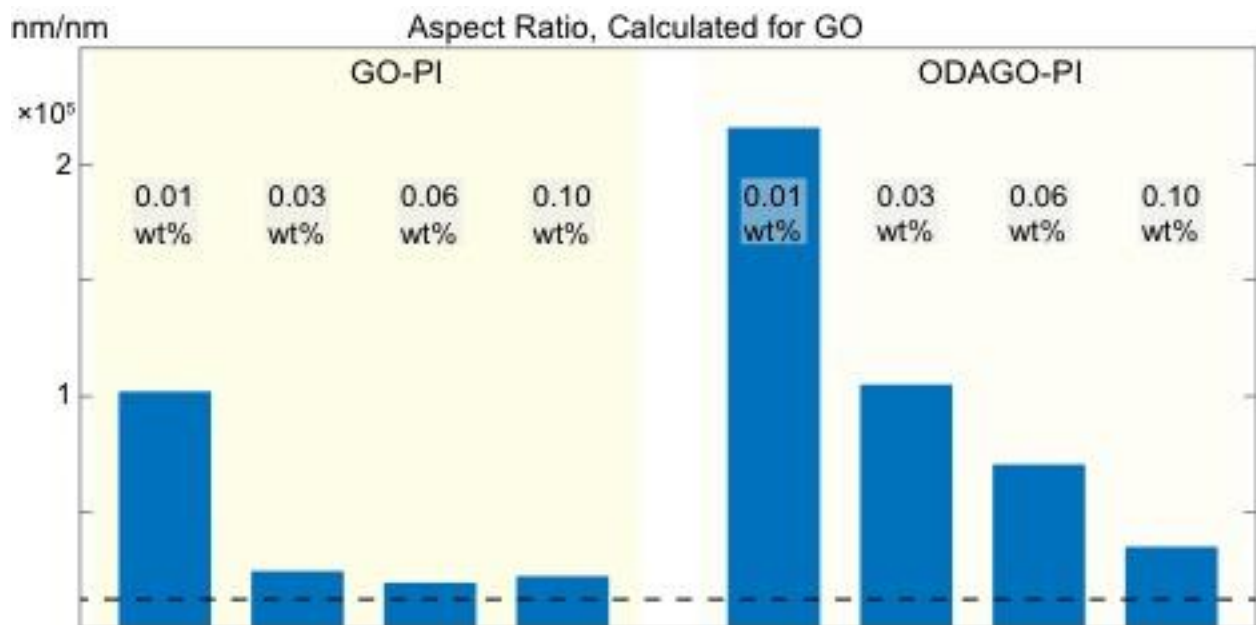


Figure 5: Calculated aspect ratio of the nanoparticles in the PI nanocomposites where the dashed line is for a value of 1000, an average aspect ratio for GO.

The modeled aspect ratios are calculated to be much greater than the AFM measured aspect values, particularly at the lowest loadings. The ODAGO aspect ratios are higher than those for GO. The values decrease as the loading gets larger. The modeled aspect ratios appear to approach experimental AFM particle size measurements as the loading increases.

These results suggest another factor in addition to the tortuosity effect induced by the high aspect ratio is producing the significant reduction in permeability at the weight percent of 0.01 percent. One factor known to correlate with reduction in permeability is reduction in mobility of

the polymer chain. A reduction in chain mobility in a polymer can be examined by the effect of the nanoparticle on the crystalline and glass phase transitions. It has been shown that GO nanoparticles inhibit crystallization in clay polyamide polymers[42-49]. The effect has been described as due to an interaction of the nanoparticle's surface with the polymer chain resulting in a region of constrained polyamide chain mobility. Similar effects of GO on the crystallization of polyamide-11 have been observed in our laboratory and are a focus of ongoing work on GO's inhibiting hydrolytic degradation.

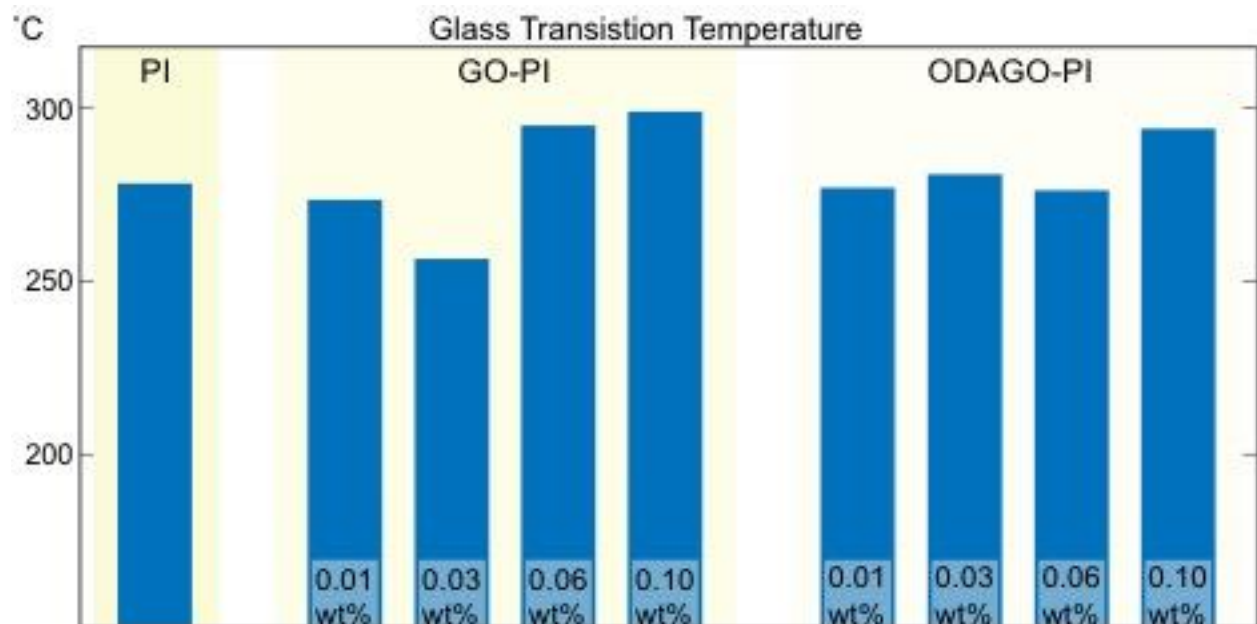


Figure 6: Glass transition temperatures (T<sub>g</sub>) of PI, GO-PI, and ODAGO-PI measured using differential scanning calorimetry.

As polyimides are amorphous glassy materials, we made measurements of the glass transition using a 30 °C/min ramp. The results in Figure 6 show an increase in T<sub>g</sub> at the highest weight percent. The nano-sheets inhibition of chain mobility as seen by an increase in T<sub>g</sub> and the effect of clay and GO nanoparticles on polyamide crystallization support the view that in addition to tortuosity, nanoparticles can inhibit chain mobility adding to the reduction in water vapor permeability.

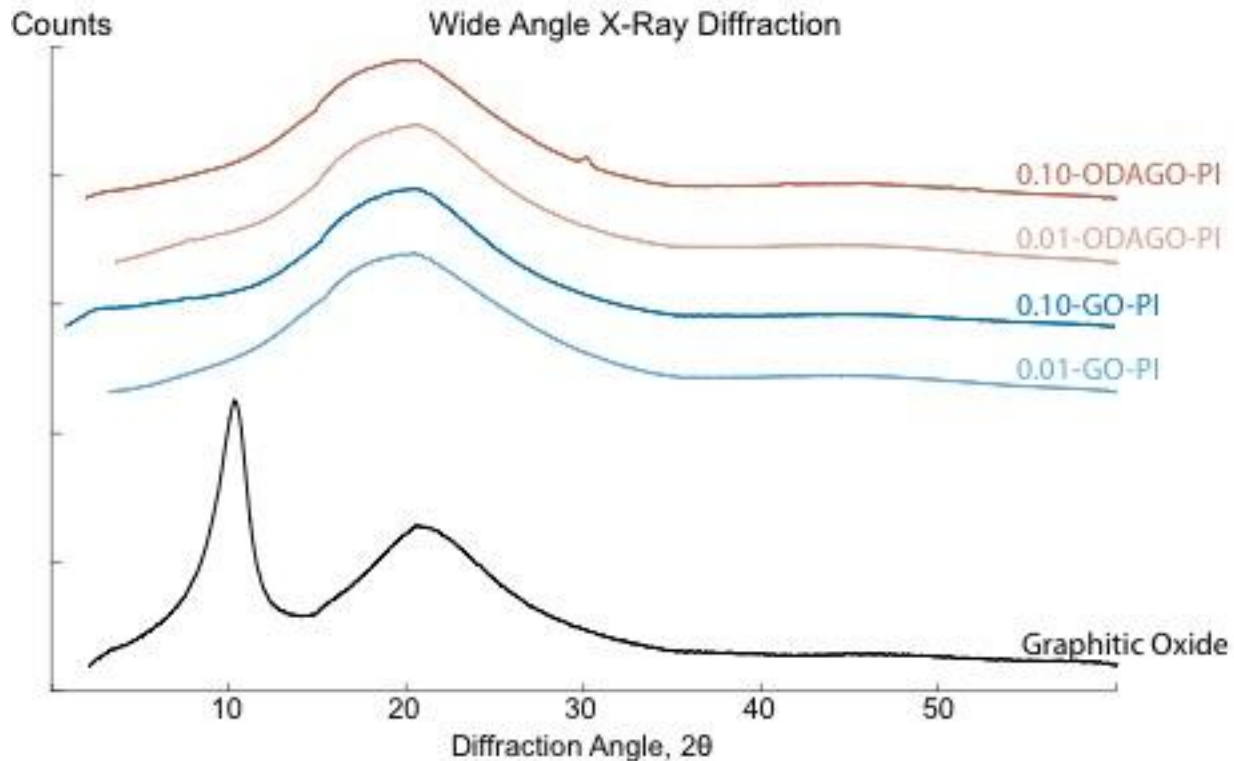


Figure 7: XRD spectra of GO, GO-PI and ODAGO-PI.

The WAXD pattern, Figure 7, for the graphitic oxide stacked GO particles had a peak at  $2\theta$  of  $11.98^\circ$  corresponding to a spacing of  $7.38 \text{ \AA}$ , which is in agreement with literature data for stacked GO sheets. The spectra for the ODAGO PI films and the GO-PI films showed only the characteristic amorphous halo, indicating[50, 51] that the ODAGO and GO nano-particles were dispersed as single sheets at these very low loadings.

The magnitude of nanoparticles affecting chain mobility would be expected to be dependent on the intermolecular interaction of the particle's surface chemistry with the chemical structure of the polymer. Thus as another means to detect the effect of the nanoparticles on the polyimide and its resulting water vapor permeability, ATR FTIR measurements were made on the neat PI film and compared with the GOPI and the ODAGOPI films as seen in Figure 8. The objective is to assess detectable interaction of the graphene nanoparticles with the polyimide matrix and differences in the interaction between the ODAGO and the GO nanosheets.

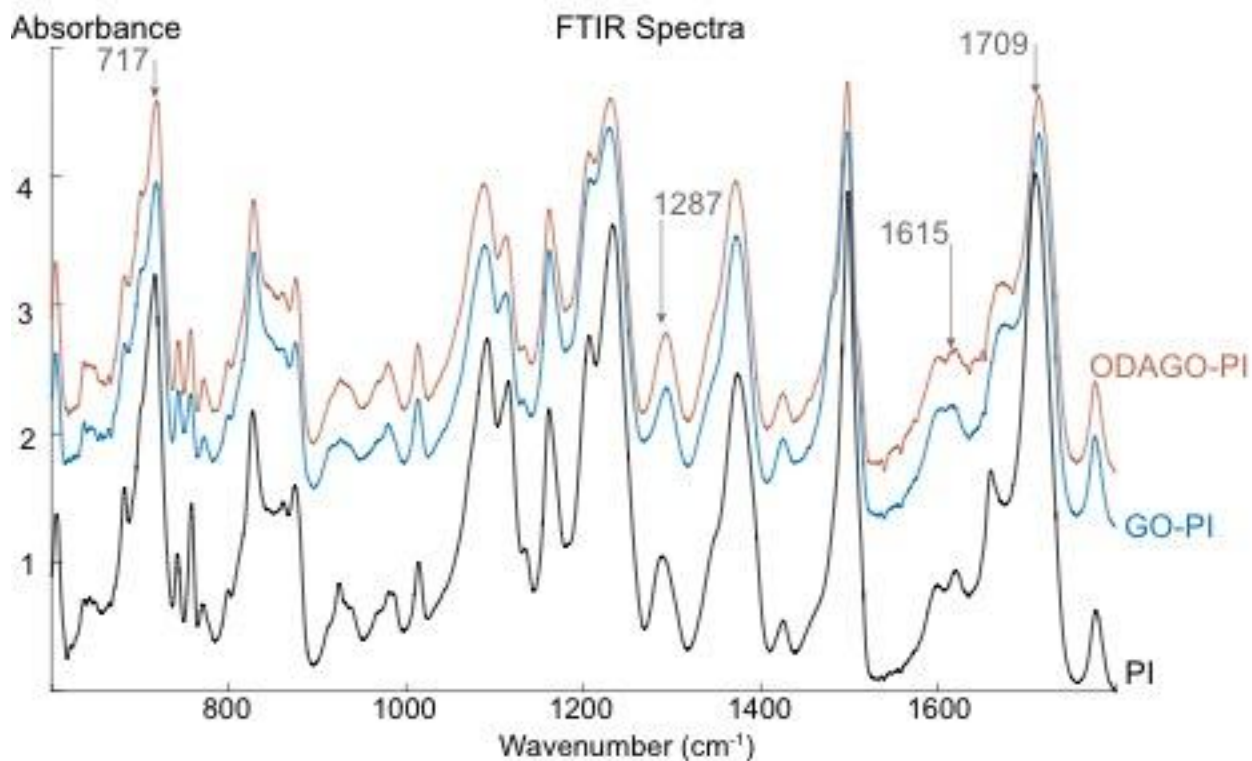


Figure 8: Fourier Transform Infrared Spectra of polyimide (PI); graphene oxide loaded PI (GO-PI) at 0.1 wt%; and ODA functionalized graphene oxide loaded PI (ODAGO-PI) at 0.1 wt%.

The known  $1615\text{--}1620\text{ cm}^{-1}$  peak for graphene's  $sp^2$  carbon structure was clearly observed in GO-PI and ODAGO-PI. Several modest shifts in the position of characteristic functional groups were observed and indicate interaction between the nanosheets and the imide bonds. The  $717\text{ cm}^{-1}$  imide ring vibration is shifted up to  $719\text{ cm}^{-1}$  for the GO-PI and up to  $720\text{ cm}^{-1}$  for the ODAGO-PI. The  $1287\text{ cm}^{-1}$  C-N imide stretch was shifted from  $1287\text{ cm}^{-1}$  for PI to  $1294\text{ cm}^{-1}$  for both GO-PI and ODAGO-PI. These results show that the C-N bond vibrates at a higher frequency in the presence of ODAGO and GO. ODAGO and GO induced a stronger C-N bond. A stronger and stiffer C-N bond indicates that the GO and ODAGO interacts with the imide ring to cause the carbon-nitrogen bond to vibrate at a higher energy and make a more rigid PI chain. The symmetric imide carboxylic oxygen stretch peak increases from  $1709$  to  $1714$  for both the GO-PI and ODAGO-PI, which indicates decreased hydrogen bonding[52, 53]. The neat

polyimide hydrogen stretch at  $3066\text{ cm}^{-1}$  was slightly down shifted to  $3064\text{ cm}^{-1}$  in the GO-PI and up-shifted to  $3069\text{ cm}^{-1}$  in the ODAGO-PI, the latter suggesting increased hydrogen interactions between the ODAGO and the PI chain than with GO and the PI chain. Finally, N-H bond stretching at  $3480\text{ cm}^{-1}$  was upshifted to  $3486\text{ cm}^{-1}$  for both the GO-PI and the ODAGO-PI, indicating hydrogen bond disruption. These results indicate that both the GO nanosheets and the functionalized ODAGO sheets are interacting with the imide ring and strengthening imide bonds in the polyimide. This produces a stiffer chain backbone and less polymer chain mobility. Evidence that ODAGO has a slightly larger effect than does GO on the chain's stiffness and resulting mobility is seen in the ODAGO's versus the GO's effect on the  $3066\text{ cm}^{-1}$  shift.

### Water Gain Analysis

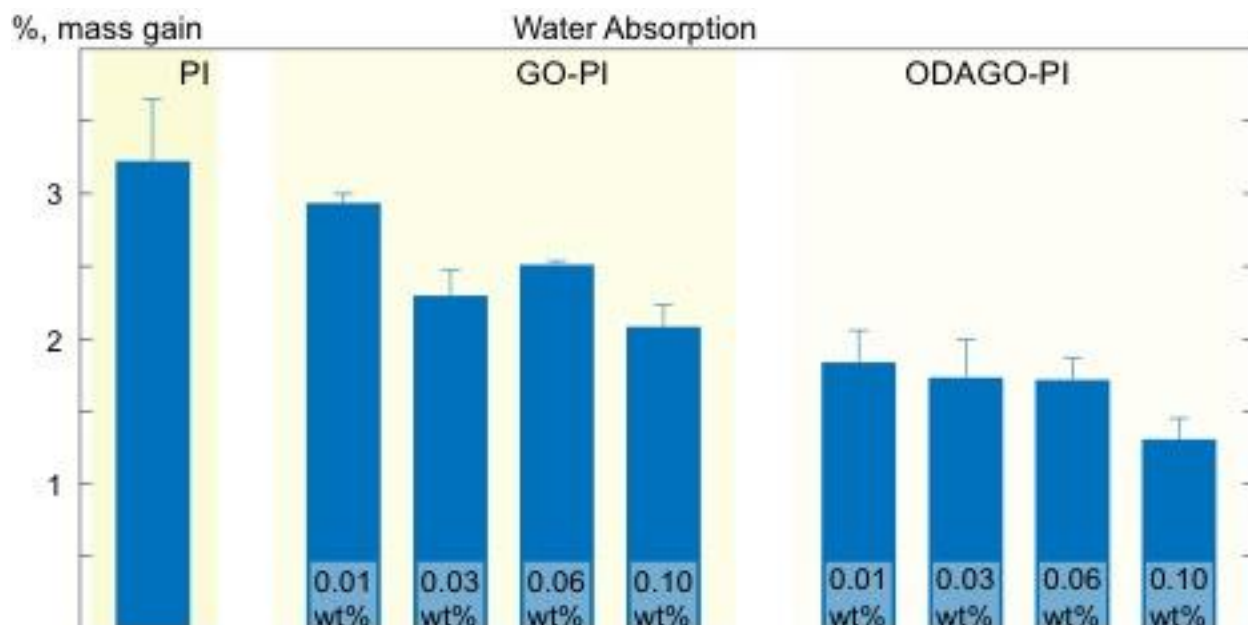


Figure 9: Percent water gain after 24 hours immersion in DI water for ODA-GO-PI, GO-PI and neat PI.

Seen in Figure 9, all GO-PI materials demonstrated less water absorption than the unloaded, neat PI film. And, functionalized ODAGO-PI had less water absorption than the GO-PI films. When compared with the neat PI 0.01 wt% ODAGO-PI had half the water absorption;

0.06 wt% ODAGO-PI absorbed a third as much water; and the 0.1 wt% ODAGO-PI absorbed two thirds as much water as the neat system.

The GO-PI system demonstrated only a 10% reduction in water absorption compared to the neat system at 0.01 wt%. At 0.06 wt% the GO-PI system demonstrated a 20% reduction in water absorption compared to the unloaded film. And, the 0.1 wt% GO-PI demonstrated a 40% reduction in water absorption compared to the unloaded film. The ODAGO loaded films demonstrate higher resistance to water absorption than films loaded with unmodified GO. Thus reacting GO with ODA is more effective in producing GO nanoparticles that improve the hydrophobic properties of the PI system.

### *Mechanical Properties*

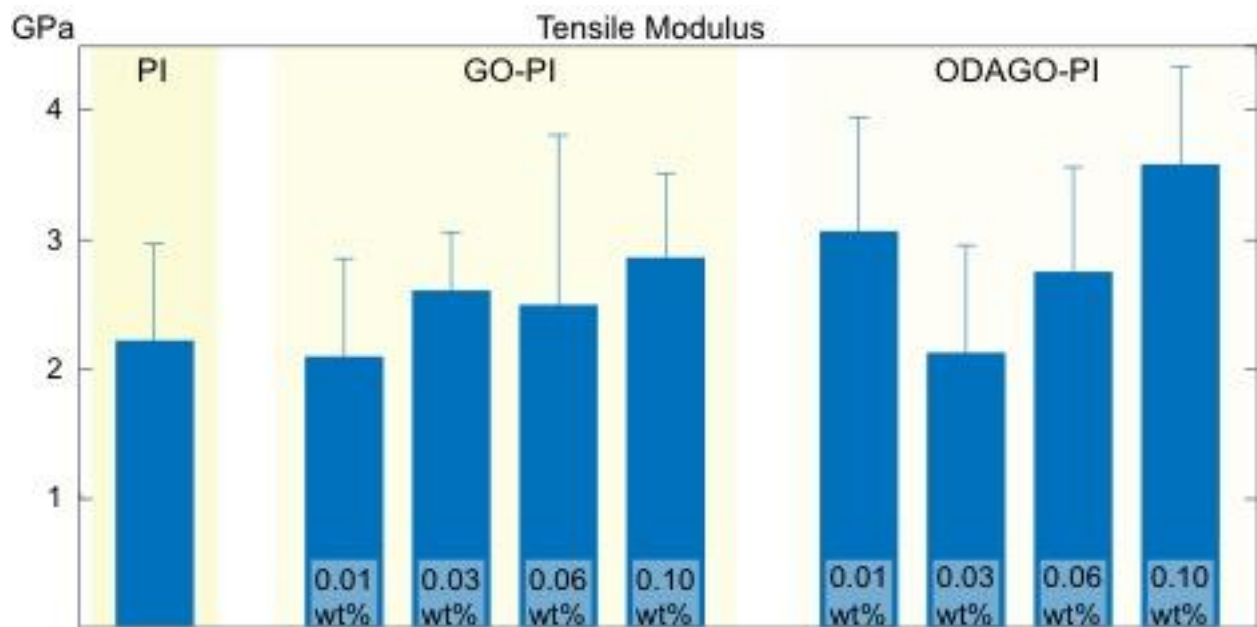


Figure 10: Young's modulus of ODA-GO-PI, GO-PI and neat PI films.

In Figure 10, Young's modulus of the PI film increased with the addition of both ODA-GO and GO nanoparticles. The Young's modulus was most effectively increased by the addition of functionalized ODAGO nanoparticles. At 0.01 wt% ODAGO-PI had an average Young's

modulus of 3.3 GPa, a 45% increase compared to the neat film. At 0.06 wt% ODAGO-PI film exhibited a Young's modulus of 2.8 GPa, a 22% increase. At 0.1 wt% ODAGO-PI increased 82% to a Young's modulus of 4.1 GPa.

The increase in Young's modulus was less in the GO-PI films. At 0.01 wt% GO-PI, Young's modulus was slightly less than neat PI. At 0.03 wt% GO-PI, Young's modulus increased 16% compared to the neat PI. The 0.06 wt% GO-PI gained 11% in the Young's modulus. The 0.1 GO-PI demonstrated an increase in the Young's modulus of 27%.

At low loadings, the Young's modulus increases for loaded PI are best achieved by using the functionalized nanoparticle, ODAGO. We attribute the improved effect of functionalized GO on tensile modulus to the surface chemistry of the GO being similar to the polymer and thereby increasing particle-polymer intermolecular forces resulting in an increase in chain stiffness. In 2011, Wang et al. [23] found a 6.6-fold improvement in the Young's modulus at 0.3 wt% ODAGO-PI and a 15-fold increase at 3 wt% ODAGO-PI, but using 3 to 300 times more ODAGO.

## CONCLUSION

Significant improvement in performance properties, most significantly in reduction of water vapor transmission is possible at GO loadings of 0.01 weight percent, a factor of ten lower than the vast majority of GO results in the literature and a factor of over one hundred lower than most gas barrier results using organo-clays.

Functionalizing the surface chemistry of the GO results in up to twice the improvement in gas barrier properties compared with un-functionalized GO-PI. The key is selecting a functionalizing molecule that readily reacts with the epoxy groups on the surface of the GO and which creates strong intermolecular attractive forces between the GO surface and the polymer. The resulting increase in particle polymer interaction is shown to stiffen the chain, reduce its mobility, and significantly enhance the tortuosity effect.

Water vapor permeability measurements to quantify gas barrier properties, water gain analysis to quantify resistance to fluids, and mechanical tensile tests all show that very low GO loadings of one part per ten thousand improve significantly these performance properties. The largest improvements occurred using ODAGO. The 0.01 wt% ODAGO-PI film demonstrated a large, 10 fold decrease in water vapor permeability. The 0.10 wt% ODAGO-PI film displayed increases of 82% in the modulus. The 0.06% functionalized GO-ODA PI film showed the largest 73% decrease in water absorption.

A much larger aspect ratio than observed using AFM measurements was calculated based on the Nielsen equation. This is shown to occur due to the additional effect of ODAGO and GO interacting with the polymer chain backbone, increasing the polyimide chain stiffness and thus decreasing mobility. The magnitude of constrained polyimide mobility diminished with

increasing nanoparticle concentration and the effective aspect ratio approached the AFM measured value at the highest concentration. The constrained mobility effect on a per particle basis was strongest at the most dilute concentration. Here, the nanosheet surface is surrounded by polyimide chains increasing particle polymer intermolecular interactions and minimizing particle–particle interaction. The nanoparticle surface interaction with the imide bond of the polyimide, constraining molecular mobility, resulted in the large unexpected reduction in water vapor diffusion, water absorption and an increase in the modulus at a very low loading of only 0.01%, one part per ten thousand, adding significantly to the nanoparticles’ high aspect ratio and high modulus.

## **AUTHOR INFORMATION**

### **Corresponding Author**

\*Telephone: (757) 221-2542. Fax: (757) 221-2050. Email: dekran@wm.edu

## **ACKNOWLEDGMENT**

NVHS thanks the Virginia Space Grant Consortium and the Charles Center of the College of William & Mary. HCS acknowledges support through the National Science Foundation, Award # DMR-1352542. DEK acknowledges the American Chemical Society’s Petroleum Research Fund Grant 542353-ND-7 for their support and funding of this project.

The authors would like to thank Professor Robert Pike for his role gathering in the x-ray diffraction spectra. Dr. Laura Dickinson for her atomic force microscopy imaging. And, Joo Yeon Roh for her help in taking Raman spectra.

## REFERENCES

1. DuPont. DuPont Electronic Materials 2015.
2. DuPont. 2015.
3. DuPont. 2013.
4. Kim H, Abdala AA, and Macosko CW. *Macromolecules* 2010;43(16):6515-6530.
5. Brodie BC. *Philosophical Transactions of the Royal Society of London* 1859;149(0):249-259.
6. Hummers Jr WS and Offeman RE. 1958:1339.
7. Chee WK, Lim HN, Huang NM, and Harrison I. *Rsc Advances* 2015;5(83):68014-68051.
8. Hu KS, Kulkarni DD, Choi I, and Tsukruk VV. *Progress in Polymer Science* 2014;39(11):1934-1972.
9. Maheshkumar KV, Krishnamurthy K, Sathishkumar P, Sahoo S, Uddin E, Pal SK, and Rajasekar R. *Polymer Composites* 2014;35(12):2297-2310.
10. Mittal G, Dhand V, Rhee KY, Park SJ, and Lee WR. *Journal of Industrial and Engineering Chemistry* 2015;21:11-25.
11. Mittal V. *Macromolecular Materials and Engineering* 2014;299(8):906-931.
12. Pan L, Liu YT, and Xie XM. *Acta Polymerica Sinica* 2014(6):724-736.
13. Potts JR, Dreyer DR, Bielawski CW, and Ruoff RS. *Polymer* 2011;52(1):5-25.
14. Saravanan N, Rajasekar R, Mahalakshmi S, Sathishkumar T, Sasikumar K, and Sahoo S. *Journal of Reinforced Plastics and Composites* 2014;33(12):1158-1170.
15. Tjong SC. *Materials Science & Engineering R-Reports* 2013;74(10):281-350.
16. Yoo BM, Shin HJ, Yoon HW, and Park HB. *Journal of Applied Polymer Science* 2014;131(1):39628-39651.
17. Zhang L, Wu JT, and Jiang L. *Progress in Chemistry* 2014;26(4):560-571.
18. Shi H, Li Y, Guo T, and Shi H. *Journal of Applied Polymer Science* 2012;128(5):3163-3169.
19. Zhu J, Lim J, Lee C-H, Joh H-I, Kim HC, Park B, You N-H, and Lee S. *Journal of Applied Polymer Science* 2014;131:40177-40184.
20. Park O-K, Kim S-G, You N-H, Ku B-C, Hui D, and Lee JH. *Composites Part B* 2014;56:365-371.
21. Chang KC. *Express Polymer Letters* 2014;8:243-255.
22. Heo C and Chang J-H. *Solid State Sciences* 2013;24(C):6-14.
23. Wang J-Y, Yang S-Y, Huang Y-L, Tien H-W, Chin W-K, and Ma C-CM. *Journal of Materials Chemistry* 2011;21(35):13569-13575.

24. Tseng IH, Liao YF, Chiang JC, and Tsai MH. *Materials Chemistry and Physics* 2012;136(1):247-253.
25. Qian Y, Wu HF, Yuan DZ, Li X, Yu WT, and Wang CY. *Journal of Applied Polymer Science* 2015;132(44).
26. Wang CY, Lan YF, Yu WT, Li X, Qian Y, and Liu HS. *Applied Surface Science* 2016;362:11-19.
27. Naebe M, Wang J, Amini A, Khayyam H, Hameed N, Li LH, Chen Y, and Fox B. *Scientific Reports* 2014;4:1-7.
28. Park YT, Qian Y, Chan C, Suh T, Nejhad MG, Macosko CW, and Stein A. *Advanced Functional Materials* 2014;25(4):575-585.
29. Shen B, Zhai W, Tao M, Lu D, and Zheng W. *Composites Science and Technology* 2013;77(C):87-94.
30. Wan Y-J, Tang L-C, Gong L-X, Yan D, Li Y-B, Wu L-B, Jiang J-X, and Lai G-Q. *Carbon* 2014;69(C):467-480.
31. Lim J, Yeo H, Goh M, Ku BC, Kim SG, Lee HS, Park B, and You NH. *Chemistry of Materials* 2015;27(6):2040-2047.
32. Cao L, Sun QQ, Wang HX, Zhang XX, and Shi HF. *Composites Part a-Applied Science and Manufacturing* 2015;68:140-148.
33. Glover AJ, Schniepp HC, Kranbuehl DE, Cai M, and Overdeep KR. *Macromolecules* 2011;44(24):9821-9829.
34. Kwon K and Chang JH. *Journal of Composite Materials* 2015;49(24):3031-3044.
35. Southward RE, Boggs CM, Thompson DW, and St Clair AK. *Chemistry of Materials* 1998;10(5):1408-1421.
36. Hain MS, Fukuda Y, Ramirez CR, Winer BY, Winslow SE, Pike RD, and Bebout DC. *Crystal Growth & Design* 2014;14(12):6497-6507.
37. Nemours EIdPd. Summary of Properties for Kapton Polyimide Films. vol. 2015. <http://www.dupont.com/content/dam/assets/products-and-services/membranes-films/assets/DEC-Kapton-summary-of-properties.pdf>. DuPont, 2015. pp. Summary of Properties for Kapton Polyimide Films.
38. Roh JY, Matecki MK, Svoboda SA, and Wustholz KL. *Analytical Chemistry* 2016;88(4):2028-2032.
39. Kudin KN, Ozbas B, Schniepp HC, Prud'homme RK, Aksay IA, and Car R. *Nano Letters* 2008;8(1):36-41.
40. Picard E, Gérard JF, and Espuche E. *Oil & Gas Science and Technology – Revue d'IFP Energies nouvelles* 2015;70(2):237-249.
41. Nielsen LE. *Journal of Macromolecular Science: Part A - Chemistry* 1967;1(5):929-942.
42. He XF, Yang J, Zhu LC, Wang B, Sun GP, Lv PF, Phang IY, and Liu TX. *Journal of Applied Polymer Science* 2006;102(1):542-549.

43. Homminga DS, Goderis B, Mathot VBF, and Groeninckx G. *Polymer* 2006;47(5):1630-1639.
44. Kolesov I, Kaci M, Lebek W, Mileva D, Benhamida A, Focke W, and Androsch R. *Colloid and Polymer Science* 2013;291(11):2541-2549.
45. Ma YL, Hu GS, Ren XL, and Wang BB. *Materials Science and Engineering a-Structural Materials Properties Microstructure and Processing* 2007;460:611-618.
46. Miltner HE, Van Assche G, Pozsgay A, Pukanszky B, and Van Mele B. *Polymer* 2006;47(3):826-835.
47. Weng WG, Chen GH, and Wu DJ. *Polymer* 2003;44(26):8119-8132.
48. Zhang Q, Yu M, and Fu Q. *Polymer International* 2004;53(12):1941-1949.
49. Zhang YS, Wang BB, and Hu GS. *Journal of Applied Polymer Science* 2012;123(1):273-279.
50. Schniepp HC, Li J-L, McAllister MJ, Sai H, Herrera-Alonso M, Adamson DH, Prud'homme RK, Car R, Saville Da, and Aksay Ia. *The journal of physical chemistry. B* 2006;110:8535-8539.
51. McAllister MJ, Li J-L, Adamson DH, Schniepp HC, Abdala AA, Liu J, Herrera-Alonso M, Milius DL, Car R, Prud'homme RK, and Aksay IA. *Chemistry of Materials* 2007;19(18):4396-4404.
52. Ma XY, Kang CQ, Chen WH, Jin RZ, Guo HQ, Qiu XP, and Gao LX. *Journal of Polymer Science Part a-Polymer Chemistry* 2016;54(4):570-581.
53. Li BY, Pang YW, Fan C, Gao J, Wang X, Zhang CL, and Liu XY. *Journal of Applied Polymer Science* 2014;131(13):9.